Structural organization of the major subunits in cyanobacterial photosystem 1 - Localization of subunits PsaC, -D, -E, -F, and -J

Kruip, Jochen; Chitnis, Parag R.; Lagoutte, Bernard; Rögner, Matthias; Boekema, Egbert J.

Published in:
The Journal of Biological Chemistry

DOI:
10.1074/jbc.272.27.17061

Publication date:
1997

THE JOURNAL OF BIOLOGICAL CHEMISTRY
Vol. 272, No. 27, Issue of July 4, pp. 17061–17069, 1997

Printed in U.S.A.

Structural Organization of the Major Subunits in Cyanobacterial Photosystem 1

LOCALIZATION OF SUBUNITS PsaC, -D, -E, -F, AND -J*

(Received for publication, January 31, 1997, and in revised form, April 25, 1997)

Jochen Kruip‡§, Parag R. Chitnis¶‖, Bernard Lagoutte, Matthias Rögner‡ ‡‡, and Egbert J. Boekema§§¶¶**

*From the ‡Institute of Botany, University of Münster, Schlossgarten 3, D-48149 Münster, Germany, the §§Groningen Biomolecular Sciences and Biotechnology Institute, Department of Biophysical Chemistry, University of Groningen, Nijenborgh 4, NL-9747 AG Groningen, The Netherlands, the **Service de Bioénergetique, Département de Biologie Cellulaire et Moléculaire, Commissariat à l'Energie Atomique, Saclay, 91191 Gif sur Yvette Cedex, France, and the ¶Department of Biochemistry and Biophysics, Iowa State University, Ames, Iowa 50011*

Based on an improved isolation procedure using perfusion chromatography, trimeric Photosystem 1 (PS1) complexes have been isolated from various deletion mutants of the mesophilic cyanobacterium *Synechocystis* PCC 6803. These mutants are only deficient in the deleted subunits, which was carefully checked by high resolution gel electrophoresis in combination with immunoblotting. These highly purified and well characterized PS1 particles were then examined by electron microscopy, followed by computer-aided image processing with single particle averaging techniques as described earlier (Kruip, J., Boekema, E. J., Bald, D., Boonstra, A. F., and Rögner, M. (1993) *J. Biol. Chem.* 268, 23353–23360). This precise methodological approach allowed a confident localization of the PS1 subunits PsaC, -D, -E, -F, and -J; it also shows shape and size of these subunits once integrated in the PS1 complex. Subunits PsaC, -D, and -E form a ridge on the stromal site, with PsaE toward the edge of each monomer within the trimer and PsaD extending toward the trimeric center, leaving PsaC in between. PsaF (near PsaE) and PsaJ are close together on the outer edge of each monomer; their proximity is also supported by chemical cross-linking, using the zero-length cross-linker EDC. This localization of PsaF contradicts the position suggested by the published low resolution x-ray analysis and shows for the first time the existence of at least one transmembrane α-helix for PsaF. A topographic three-dimensional map has been drawn from this set of results showing the location of the major PS1 subunits (besides PsaA and PsaB). These data also led to the assignment of electron density in the recent medium resolution x-ray structure for PS1 (Krauss, N., Schubert, W.-D., Klukas, O., Fromme, P., Witt, H. T., Saenger, W. (1996) *Nat. Struct. Biol.* 3, 965–973).

Photosystem 1 (PS1)[1] is one of the two transmembrane pigment-protein complexes of oxygenic photosynthesis located in the thylakoid membrane of chloroplasts and cyanobacteria. Its main function is the light-dependent electron transfer from plastocyanin (or cytochrome c_6) on the lumen side to soluble ferredoxin (or flavodoxin) on the cytoplasmic or stroma side, thereby transforming light energy into reducing power for various biosynthetic pathways (see Refs. 1–3 for reviews). Cyanobacterial PS1 consists of 11 subunits, named PsaA to PsaM, with PsaG and PsaH missing, as they are found only in chloroplasts (3); all their sequences are known (1). The hydrophilic subunits PsaC, -D, and -E are localized on the cytoplasmic side (4), and PsaF is supposed to sit on the lumenal side of the thylakoid membrane. All the other subunits are integral membrane proteins.

In terms of function the initial steps of light harvesting and charge separation are carried out by only three proteins. The PsaA/PsaB heterodimer harbors the primary electron donor P700 (a chlorophyll dimer) and the electron acceptors A_0 (a monomeric chlorophyll), A_1 (a phylloquinone), and F_X (a [4Fe4S] iron-sulfur cluster) in addition to about 100–130 antenna chlorophyll molecules (5). PsaC contains the terminal electron acceptors F_A and F_B (both [4Fe4S] iron-sulfur clusters). The other proteins do not bind any cofactors, but fulfill important functional and structural roles: PsaD and -F have been shown to be candidates for ferredoxin (6, 7) and plastocyanin docking (8, 9), respectively. PsaE plays an important role in cyclic electron flow (10) and ferredoxin reduction (11, 12), while PsaL and PsaD are important for trimer formation (4, 13, 14).

To elucidate the function of all subunits on a molecular level, a high resolution structure is necessary. Despite several crystallization reports (15–17), a low-resolution x-ray analysis (6 Å) for PS1 from the thermophilic cyanobacterium *Synechococcus elongatus* became available only in 1993 (18). Recently this x-ray analysis was extended to 4 Å (19, 57). In this study, 31 transmembrane, 9 surface, and 3 stromal α-helices, 65 chlorophyll *a* molecules, and three [4Fe4S] clusters could be fitted into the electron density map. Due to the medium resolution it is not possible to attribute the identified structural elements

* The costs of publication of this article were defrayed in part by the payment of page charges. This article must therefore be hereby marked "*advertisement*" in accordance with 18 U.S.C. Section 1734 solely to indicate this fact.

§ Present address: Research Laboratory for Resources Utilization, Tokyo Institute of Technology, 4259 Nagatsuta, Yokohama 226, Japan.

‖ Supported by the National Science Foundation, National Institutes of Health, and United States Department of Agriculture.

‡‡ Supported by the Deutsche Forschungsgemeinschaft and Research Institute of Innovative Technology for the Earth. To whom correspondence should be addressed. New address: Lehrstuhl für Biochemie der Pflanzen, Fakultät für Biologie, Ruhr-Universität Bochum, D-44780 Bochum, Germany. Tel.: 49-234-700-3634; Fax: 49-234-7094-322; E-mail: matthias.roegner@rz.uni-bochum.de.

¶¶ Supported by European Community Grant 2CT930087.

[1] The abbreviations used are: PS, Photosystem; DMP, dimethylpimedilate; EDC, *N*-ethyl-3-(3-dimethylaminopropyl)carbodiimide; EM, electron microscopy; NHS, *N*-hydroxysulfosuccinimide; β-DM, dodecyl-β-D-maltoside; PAGE, polyacrylamide gel electrophoresis; PCC, Pasteur Culture Collection; Psa, photosystem 1 protein (PS 1 nomenclature); WT, wild type; MES, 4-morpholineethanesulfonic acid; HPLC, high performance liquid chromatography.

TABLE I
Synechocystis sp. PCC 6803 deletion strains used in this study

Strain	Description	Ref.
WT	Glucose-tolerant wild type strain.	(56)
AFK6	*psaF* replaced by a kanamycin resistance cartridge. *psaJ* transcriptionally inactivated.	(49)
AJC8–3	*psaF* reintroduced into AFK6 strain. *psaJ* replaced by a chloramphenicol resistance gene.	(30)
ALC7–3	*psaL* replaced by a chloramphenicol resistance gene.	(52)
DE	*psaD* and *psaE* genes replaced by genes for chloramphenicol and kanamycin resistance, respectively.	(13)
FKE2	*psaE* replaced by a kanamycin resistance cartridge.	(12)
KDB3	*psaD* replaced by a kanamycin resistance gene.	(24)

unambiguously (without additional information) to specific subunits.

Previously, we have shown the possibility to determine the position of individual subunits within the PS1 complex and also the docking position of the electron acceptor proteins flavodoxin and ferredoxin by electron microscopy in combination with single particle averaging techniques (4, 20, 21). The availability of several deletion mutants (Table I) now enables the extension of these studies to a nearly complete structural analysis of the location of the major subunits of PS1, indicating clearly the position of subunits PsaC, -D, -E, -F, and -J within PS1. In combination with cross-linking data, these electron microscopy data lead to the development of a new topographical map for the location of the structurally and functionally most important subunits of PS1. The excellent resolution of these data was also supported by a major improvement (regarding purification time) of the chromatographic isolation procedure for PS1 using perfusion chromatography; the versatility of this method for speeding up the purification of membrane proteins in general is shown.

MATERIALS AND METHODS

Isolation of PS1 Complexes—Growth conditions of *Synechocystis* sp. PCC 6803 and subsequent isolation of thylakoid membranes were described earlier (22). Also, the purification strategy for the isolation of extremely pure monomeric and trimeric PS1 complexes from these membranes involving HPLC was outlined before (4). However, for the results of this paper we replaced the anion exchange step using "conventional" HPLC by an anion exchange step based on perfusion chromatography. A detailed comparison of perfusion chromatography and conventional HPLC will be published elsewhere. Briefly, after obtaining fractions enriched in monomeric or trimeric PS1 by sucrose gradient centrifugation, sucrose was removed by ultrafiltration, and the resulting solution (1 mg of chlorophyll/ml) was applied onto an anion exchange perfusion column (Poros 50 HQ 10/100; Perseptive, Wiesbaden, Germany) and eluted by a linear gradient of $MgSO_4$ (5–200 mM). Upon exchange of buffer the material was further purified by a hydroxyapatite HPLC chromatography (Superformance hydroxyapatite 50–10; Merck, Darmstadt, Germany). Perfusion chromatography columns were run in a Waters HPLC system consisting of two pumps 510, a controller 680, and a dual wavelength detector (as described in Ref. 4).

Rebinding of PsaC—Refolded PsaC (which has been overexpressed in an *Escherichia coli* strain) was a kind gift of Dr. J. Golbeck (University of Nebraska, Lincoln, NE). Rebinding assays with purified trimeric PS1 lacking subunits PsaC/D/E (isolated from the DE strain) were done overnight according to (23) with the exception that PsaD and PsaE were omitted. Immediately before EM analysis, the buffer was exchanged (see EM part) by repeated ultrafiltration (MicroCon (100-kDa cutoff), Amicon, Witten, Germany).

Cross-linking of PS1 Subunits within the Membrane—Isolated thylakoid membranes from the KBD3 strain (24) were treated with the cross-linker DMP at a chlorophyll concentration of 1 mg/ml in HEPES buffer (20 mM HEPES (pH 7.5), 10 mM $MgCl_2$, 10 mM $CaCl_2$ for 2 h at 4 °C. DMP was added in three steps (intervals of 20 min) to a final concentration of 20 mM. The reaction was stopped by the addition of ammonium acetate to a final concentration of 50 mM. Membranes were pelleted and washed several times before extraction. Trimeric PS1 complexes were isolated as described above.

Cross-linking of Subunits within Isolated PS1 Complexes—Isolated PS1 complexes (10 μg of chlorophyll, reaction volume 300 μl) were incubated for 30 min at room temperature in an assay consisting of 4 mM EDC, 4 mM sulfo-NHS, 20 mM HEPES (pH 7.5), 5 mM $MgCl_2$, and 0.03% (w/v) β-DM. The reaction was stopped by the addition of ammonium acetate to a final concentration of 50 mM. Prior to SDS-PAGE analysis the PS1 complexes were washed several times with 20 mM MES (pH 6.8), 10 mM $MgCl_2$, 10 mM $CaCl_2$, and 0.03% (w/v) β-DM by ultrafiltration (MicroCon with 100-kDa membrane; Amicon).

Preparation of Fab-labeled PS1—Anti-PsaD antibodies were purified from crude serum by ammonium sulfate precipitation followed by anion exchange chromatography (Poros HQ/M; Perseptive). Fab fragments were generated using the ImmunoPure Fab preparation kit (Pierce, Oud-Beijerland, Netherlands) according to instructions supplied by the manufacturer. Binding to trimeric WT PS1 was done overnight at 4 °C in Tris-buffered saline (pH 7.8). The material was immediately examined with EM.

Biochemical Standard Techniques—SDS-PAGE was done according to Schaegger and von Jagow (4). For immunoblotting the proteins were electroblotted (Fastblot; Biometra, Göttingen, Germany) onto a polyvinylidene difluoride membrane (Immobilon; Millipore). Immunochemical detection using a secondary alkaline phosphatase-coupled antibody was carried out as described in Ref. 22. Antibodies against the PsaC, -D, and -E proteins were kindly provided by Dr. J. Golbeck (University of Nebraska). Chlorophyll concentrations were determined using an extinction coefficient of 74,000 M^{-1} cm^{-1} at 679 nm.

Electron Microscopy and Image Analysis—PS1 complexes, equilibrated in MES buffer (10 mM MES (pH 6.8), 5 mM $MgCl_2$, 5 mM $CaCl_2$, and 0.02% β-DM) by overnight dialysis, were prepared for EM using the droplet method with 2% uranyl acetate as negative stain. During the staining procedure the grid was washed once with distilled water for several seconds to reduce detergent aggregation in the background. EM was performed with a JEOL JEM 1200-EX electron microscope at × 60,000 magnification. Micrographs were digitized with a Kodak Eikonix model 1412 CCD camera with a step size of about 25 μm, corresponding to a pixel size of 0.45 nm at the specimen level. Single particle analysis was performed on a Silicon Graphics Indy workstation. We followed the alignment strategy and further analysis methods as used previously (25, 26). First the images were pretreated to normalize the variance, then they were windowed with a circular mask. A band pass, suppressing the highest and lowest frequencies of the images, was imposed on the particles in the alignment step. In the next steps the projections were treated with multivariate statistical analysis in combination with classification (27, 28). In the classification step, 10–15% of the images were automatically rejected. Finally, sums of projections belonging to the various classes were made by adding up the original images without band-pass filter. For these final sums, the best 50–70% of the class members were taken, with the correlation coefficient in the alignment procedure as the quality criterion.

Materials—β-DM was purchased from Biomol (Hamburg, Germany), 4 mM *N*-ethyl-3-(3-(dimethylamino)-propyl)-carbodiimide (EDC), and 4 mM sulfo-NHS from Fluka (Deisenhofen, Germany), and DMP from Sigma (Deisenhofen, Germany). Most other chemicals and antibiotics were purchased from Sigma.

RESULTS

Isolation of Different PS1 Complexes—Based on an already existing method for the purification of PS1 complexes, which yielded pure and homogeneous monomeric and trimeric PS1 complexes by several HPLC steps (4, 22), we succeeded in speeding up the isolation procedure considerably by the introduction of perfusion chromatography without losing resolution or activity of the preparation. Fig. 1 shows a direct comparison between conventional HPLC (Fig. 1*A*) and perfusion chroma-

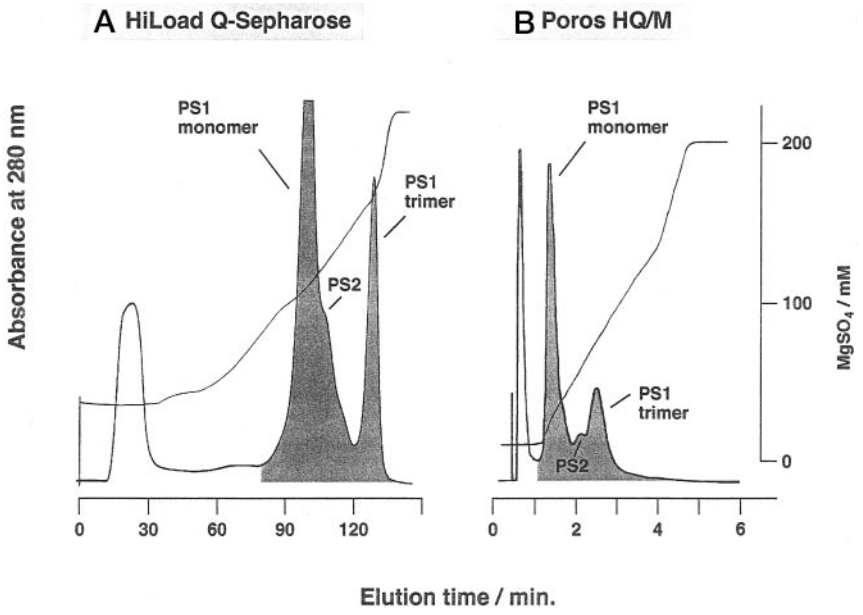

FIG. 1. **Purification of trimeric PS1 (in this case of the AFK6 mutant strain) by anion-exchange chromatography (the sample had been prepurified on a sucrose density gradient).** *A*, elution profile of a conventional anion exchange HPLC (HiLoad Q-Sepharose HP 16–10; Pharmacia Biotech Inc., Freiburg, Germany) with a $MgSO_4$ gradient (5–200 mM; *upper trace* shows conductivity) at 10 °C and a flow rate of 1 ml/min. *B*, elution profile of a perfusion chromatography anion exchange column (Poros HQ/M; Perseptive) with a linear $MgSO_4$ gradient (5–200 mM; the *upper trace* shows the measured conductivity) at 10 °C and a flow rate of 6 ml/min. In both cases absorbance was recorded at 280 nm.

tography (Fig. 1*B*) of extracted PS1 complexes, which have been applied on anion exchange columns. In both cases the mixture is resolved into four peaks, which have been identified by gel electrophoresis and absorption spectra (see also Refs. 4 and 22) as a mixture of carotenoids and phycobiliproteins (peak 1), monomeric PS1 (peak 2), monomeric PS2 (peak 3), and trimeric PS1 (peak 4), respectively. While the resolution is identical in both runs, the elution time of the respective peaks differs remarkably. Perfusion chromatography allows an about 20-fold faster separation, thus facilitating the purification of large amounts of PS1 in a short time. This isolation procedure could be applied for all PS1 deletion strains as it was found that the lack of selected PS1 subunits did not change the chromatographic properties of the respective PS1 complexes, at least not in case of the mutants studied in this report (data not shown).

Fig. 2 shows a SDS-PAGE analysis of the different PS1 complexes used in this work. In case of the PsaL deletion mutants (Fig. 2*A, lanes 2* and *3* and Fig. 2*D, lane 3*) only monomeric PS1 could be isolated (data not shown). All other mutants show the expected loss of the deleted subunits in the isolated complexes. The AFK6 mutant shows the expected loss of PsaF/J (Fig. 2*B, lane 2*) seen usually as two separate bands about 1 kDa apart (4). Even when PsaF is reintroduced into this strain (mutant AJC8-3), the amount of PsaF in isolated trimeric PS1 is still very low, yielding only about 30% of the amount in WT (Fig. 2*A, lane 4*). Isolated trimeric PS1 from the PsaD/E deletion mutant shows the additional loss of PsaC upon isolation (Fig. 2*B, lane 3*).

Fig. 2*C* shows that deletion of PsaE does not affect the stable assembly of the other subunits; the existence of the trimeric and the monomeric forms also remains unaffected by this deletion (data not shown).

Upon deletion of the PsaD subunit the vast majority of PS1 was isolated in the monomeric form. SDS-PAGE analysis (Fig. 2*D, lane 2*) shows the concomitant loss of the PsaL subunit from these particles, indicating a close vicinity of PsaD and -L. As trimeric PS1 is a prerequisite for high resolution single particle EM analysis (29) membranes have been treated (prior to extraction) with a cross-linker to stabilize the trimeric form of PS1. This treatment indeed enabled the isolation of trimeric PS1 which contained PsaL but no PsaD as verified by immunoblotting (data not shown).

Cross-linking Analysis of PS1—Cross-linking of WT PS1 with the zero-length cross-linker EDC (and sulfo-NHS) results in the formation of two major adduct bands (Fig. 3). The band centered around 35 kDa cross-reacts both with antibodies against PsaD and against PsaL (Fig. 3*A, lanes 1* and *3*). This band is absent in cross-linked PS1 particles lacking PsaD (Fig. 3*B, lane 3*) or PsaL (Fig. 3*B, lane 4*), confirming the assignment of this band as a PsaD-L adduct. There are no major differences between monomeric and trimeric PS1 (data not shown); the only exception is that in trimeric PS1 (Fig. 3*B, lane 1*) an additional cross-link product at higher molecular mass (around 60 kDa) can be detected by an anti-PsaD antibody. The other major cross-linking adduct bands (at around 25 kDa) are recognized by four different antibodies: anti-PsaD, anti-PsaC, anti-PsaE, and anti-PsaF (Fig. 3*A, lanes 3–10*). Cross-linking of PS1 lacking PsaF/J leads to a cross-link product of about 25 kDa, which is recognized only by the anti-PsaC and anti-PsaD antibodies (Fig. 3*C*); taken together, these results indicate the existence of two different cross-linking adducts, *i.e.* PsaC-D and PsaE-F, with roughly the same molecular mass recognized as only one band in SDS-PAGE.

Structural Analysis of Trimeric PS1 Complexes by Electron Microscopy—Single particle analysis was performed on projections of negatively stained trimeric particles (Fig. 4), which differed in their subunit composition due to site-directed mutagenesis (for types of mutants see Table II). Nine data sets, comprising a total of about 10,000 single projections, were analyzed. The results of this analysis are shown in Fig. 5. Each set of projections was analyzed independently by the standard procedure outlined under "Materials and Methods." Classification of the various projections (see "Materials and Methods") revealed in some cases the presence of projections differing in handedness, which previously have been termed "flip" and "flop" projections (4). However, in most data sets a large majority of the projections had the same type of handedness. Also, as already noticed before (21), many of the projections lacked a clear 3-fold symmetry due to a slight tilting of the PS1 complexes on the "rough" carbon support. Due to this tilting one out of three of the projected monomers within some trimers appears considerably smaller than the other two, and also smaller image details, such as the small connecting masses in the center of the trimer, appear to be different (21). For this reason, only 50–70% of the projections was summed of those classes showing well preserved 3-fold symmetry and clear central connecting masses. On the average, about 150 projections were used for the final sums, which then were 3-fold averaged (Fig.

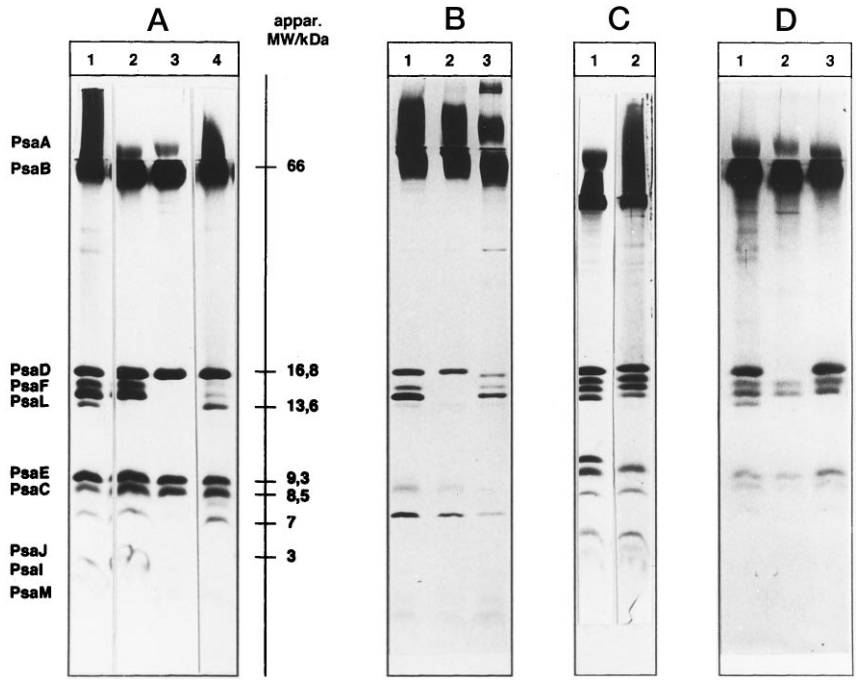

FIG. 2. **SDS-PAGE analysis (according to Ref. 4) of purified PS1 complexes used in this study.** *A*, trimeric PS1 of WT (*lane 1*), monomeric PS1 lacking PsaL (*lane 2*), monomeric PS1 lacking PsaF/J/L (*lane 3*), and trimeric PS1 lacking PsaJ (*lane 4*). *B*, trimeric PS1 of WT (*lane 1*), trimeric PS1 without PsaF/J (*lane 2*), and trimeric PS1 lacking PsaD/E (*lane 3*). *C*, trimeric PS1 of WT (*lane 1*) and monomeric PS1 lacking PsaE (*lane 2*). *D*, trimeric PS1 of WT (*lane 1*), monomeric PS1 lacking PsaD (*lane 2*), and monomeric PS1 lacking PsaL (*lane 3*). All gels were stained with Coomassie Blue.

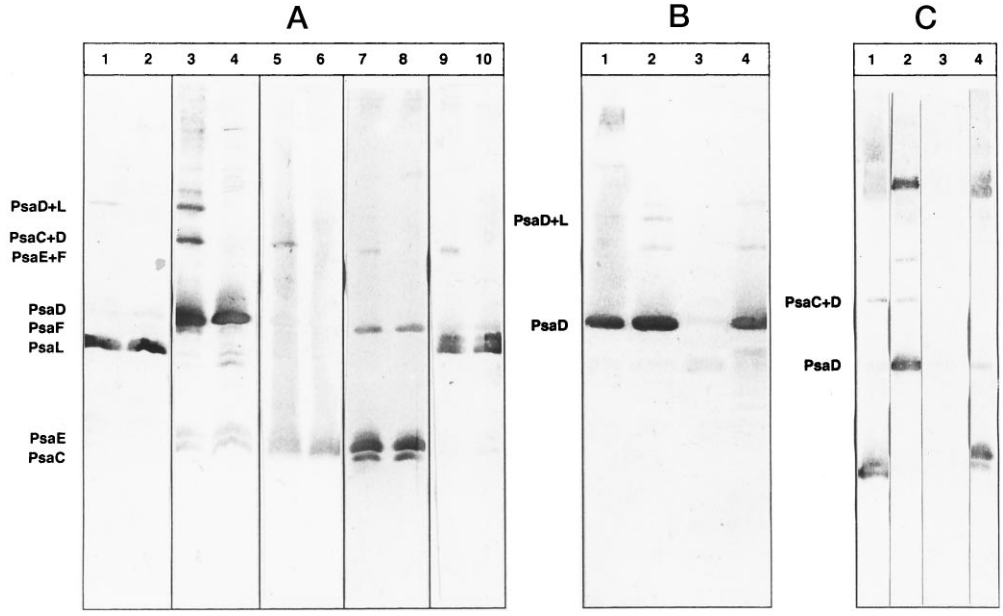

FIG. 3. **Analysis of cross-linking products by immunoblotting.** *A*, comparison of cross-linked and uncross-linked WT PS1 complexes; *even numbered lanes*, WT PS1; *odd numbered lanes*: PS1 cross-linked with EDC and sulfo-NHS. For immunodetection the following antibodies have been used: anti-PsaL (*lanes 1* and *2*), anti-PsaD (*lanes 3* and *4*), anti-PsaC (*lanes 5* and *6*), anti-PsaE (*lanes 7* and *8*), and anti-PsaF (*lanes 9* and *10*). *B*, analysis of the PsaD-L cross-link using anti-PsaD for immunodetection: *lane 1*, cross-linked trimeric WT PS1; *lane 2*, cross-linked monomeric WT PS1; *lane 3*, cross-linked PS1 lacking PsaD; and *lane 4*, cross-linked PS1 lacking PsaL. *C*, probing the PsaC-D and PsaE-F cross-link. Cross-linked trimeric PS1 lacking PsaF/J was probed with anti-PsaC (*lane 1*), anti-PsaD (*lane 2*), anti-PsaF (*lane 3*), and anti-PsaE (*lane 4*), respectively. All lanes contain 20 μg of chlorophyll.

5). From the averaged top views shown in Fig. 5, it is obvious that each mutant shows a characteristic (specific) electron density pattern.

Difference images between PS1 lacking various subunits and PS1 of WT indicate the area most likely occupied by the missing subunit(s) (Fig. 6). As particles from the DE deletion strain lose the PsaC subunit during purification (see Fig. 2), the difference view (Fig. 6*A*) indicates the area covered by subunits PsaC/D/E on the cytoplasmic side. Attempts to rebind PsaC to these particles to localize this subunit in a difference view failed (see "Discussion"), resulting in difference maps (not shown) that are nearly identical to Fig. 6*A*. Particles lacking only PsaE show the main difference (Fig. 6*C*) toward the outer edge of the monomer within the difference area of PsaC/D/E (compare with Fig. 6*A*), whereas particles deficient in PsaD miss electron density on the opposite side of this area (Fig. 6*B*). This indicates a location of PsaD toward the center of the trimer. The location of subunits PsaD and -C could also be deduced from the difference of Fig. 5, *G* and *C*. It is obvious that in addition to the area occupied by PsaD (Fig. 6*D*), the difference area extends in this case toward the center of the monomer (Fig. 6*H*), indicating the central position of PsaC.

Difference maps between PS1 of WT and PS1 lacking PsaF/J or PsaJ clearly show areas on the outer edge of each monomer,

whereas the difference views of PsaF/J and the PsaJ deletion mutant show only minor differences (Fig. 6, *E* and *F*).

To distinguish between the location of PsaF and PsaJ we analyzed material from a mutant where the PsaF gene was reintroduced. Unfortunately the absence of PsaJ destabilizes the binding of PsaF to the complex (30) in such a way that only around 30% of the purified PS1 complexes contain PsaF (as judged from SDS-PAGE, see Fig. 2*A*). Consequently, the difference area found for this mutant (Fig. 6*F*) resembles closely the area already attributed to PsaF and PsaJ (Fig. 6*F*), indicating that most of the analyzed particles had lost PsaF. The second analysis with higher resolution shows that complexes lacking PsaF/J miss an area of about 3 nm^2 in the periphery of the trimer, indicative for at least two membrane-spanning α-helices.

Analysis of Side View Projections—Trimeric PS1 complexes have a tendency to aggregate into pairs on their flat side. If the hydrophilic subunits on the cytoplasmatic side are present, this leads to side view projections in which an asymmetric gap between the "sandwich" of two trimers is visible (Fig. 4). Absence of the cytoplasmic exposed subunits leads to a strong reduction of the gap in combination with a reduced height of the whole sandwich. Aggregation of several sandwiches into small strings can also be observed (4). These aggregated side views yield a more accurate estimation of the overall height of the individual particle as it can be gained from averaging the height of many particles in the strings (Table II), resulting in about 9.2–9.3 nm for PS1 of WT. While complexes lacking PsaF and -J show only a minor reduction of the height, resulting in 8.4–9.0 nm, complexes lacking subunits PsaC/D/E have only a height of 6.7 nm (Table II). This indicates that the complex extrudes about four times more into the stroma (by subunits C/D/E) than into the lumen (by subunit F). Particles lacking either PsaD or -E show an intermediate height. The fact that particles of mutants with deleted PsaD and -E that were used for PsaC rebinding showed a similar height as particles lacking PsaC/D/E confirms the loss of PsaC during purification and is in agreement with SDS-PAGE analysis (Fig. 2).

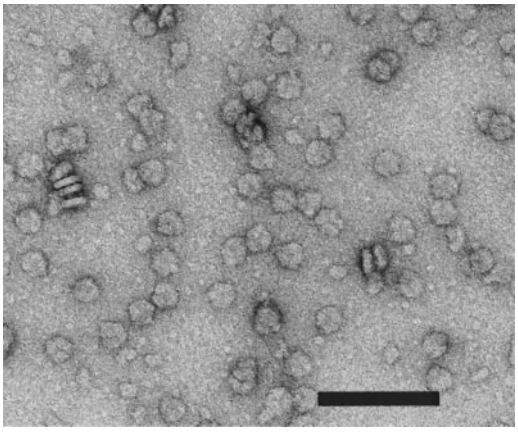

FIG. 4. **Electron microscopy of trimeric PS1 isolated from the *Synechocystis* AFK6 strain, lacking the subunits PsaF and PsaJ. The scale bar represents 100 nm.**

DISCUSSION

Purification of PS1—This paper describes a new, extremely fast chromatographic method to purify PS1 on a large scale and at a purity level suitable for crystallization. Compared with the previously published method (4, 22), the anion exchange step was speed up 20-fold: from a time range of hours to a time range of minutes. The unique properties of perfusion chromatography made this possible. The matrix used in perfusion chromatography contains large "perfusion" pores (600–800 nm in diameter), which allow rapid mass transfer to the interior of the particles. Consequently, the resolution is nearly independent of the flow rate (31). This offers easy scale up opportunities, especially important for structural work (x-ray, NMR), where large amounts of pure material are needed. Perfusion chromatography use similar surface chemistries as conventional chromatography. This makes the conversion from conventional chromatography to perfusion chromatography quite easy. The earlier elution of PS1 in the perfusion column offers an additional advantage, as it saves both time and prevents PS1 from exposure to high salt concentrations, which may lead to subunit loss. The combination of all these effects makes perfusion chromatography not only a method of choice for the rapid preparation of labile complexes (32) but also very attractive for large scale preparations of proteins, especially membrane proteins, for subsequent structural analysis.

Structural Model of PS1—The low resolution crystal structure of trimeric PS1 from *S. elongatus* published in 1993 (18) was a major step toward understanding PS1 at the molecular level. However, the 6-Å resolution obtained in this work did not allow the attribution of protein structures to specific PS1 subunits. The situation was not significantly improved by the recent resolution improvement to 4.5 Å (19, 57). Results gained in this paper, based on side-directed PS1 mutants from the cyanobacterium *Synechocystis* 6803, allow the distinct and rather precise localization of individual PS1 subunits due to differences in averaged EM images with and without these subunits. This procedure has already been outlined in detail before (29) and applied successfully by us for several membrane protein complexes (4, 20, 21). To differentiate between noise and actual signals in the generated difference maps we made an independent analysis of projections, taken from the same preparation (Fig. 5, *A* and *B*), which shows that dissimilarities in the difference image below 20% of the total signal level are due to noise (28). By taking this 20% level as the lowest contoured level in difference images (as presented in this work), areas which fall within contours are indicative for the position of the missing mass. It appears that in most difference images

TABLE II
Average dimensions of different trimeric PS1 particles

Average thickness of trimeric complexes was determined from particles aggregated in side-view position (nm) obtained either by averaging aligned images or by directly measuring distances on printed electron micrographs (for which the standard deviation is indicated).

Source of trimeric PS1	Deficient subunit according to SDS-PAGE	Diameter	Height
		nm	*nm*
WT 1		19	9.3 ± 0.3 (n = 50)
WT 2		19	9.2 ± 0.4 (n = 40)
WT (urea)	PsaC/PsaD/PsaE	19	6.7 (n = 50)
AFK6	PsaF/PsaJ	19	8.4 (n = 50)
AJC8–3	PsaJ	19	9.0 ± 0.6 (n = 74)
DE	PsaC/PsaD/PsaE	19	6.6 (n = 50)
DE (attempt to rebind PsaC)	PsaC/PsaD/PsaE	19	6.8 (n = 58)
FKE2	PsaE	19	8.6 ± 0.4 (n = 78)
KDB3	PsaD	19	7.3 ± 0.4 (n = 41)

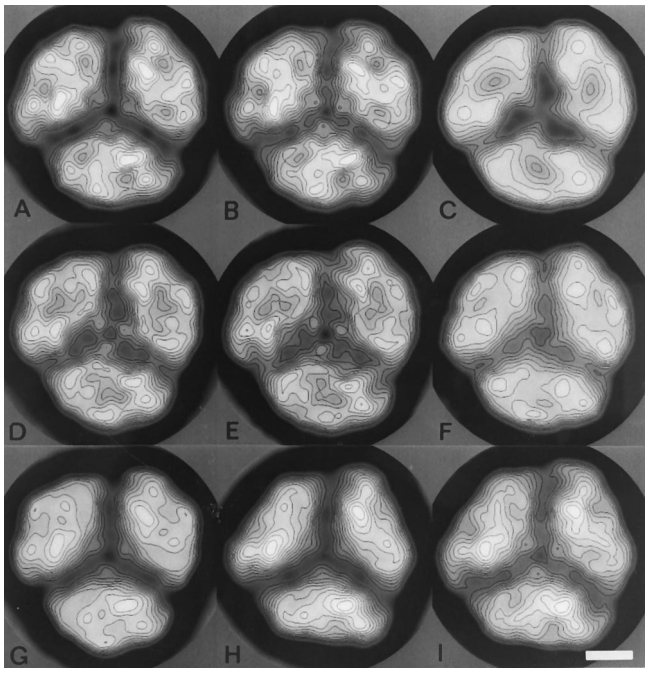

FIG. 5. **Final results of single particle averaging of trimeric *Synechocystis* 6803 PS1 projections.** *A*, sum of 114 top view images (out of 898 selected projections) of wild type PS1 complexes (modified from Ref. 4). *B*, sum of 150 top view images (out of 1464 selected projections) of a second independent analysis of WT PS1 complexes (taken from Ref. 20). *C*, sum of 125 images (out of 391 selected projections) of urea-washed complexes lacking PsaC/D/E (modified from Ref. 4). *D*, sum of 125 images (out of 947 selected images) of complexes lacking PsaD/E. *E*, sum of 200 images (out of 877 selected images) lacking PsaD/E after an attempt to rebind PsaC (see "Discussion"). *F*, sum of 80 images (out of 323 selected images) of complexes lacking PsaD. *G*, sum of 125 images (out of 1345 selected images) of complexes lacking PsaE. *H*, sum of 340 images (out of 1332 selected images) of complexes lacking PsaF/J. *I*, sum of 150 images (out of 1900 selected images) of complexes lacking PsaJ. All images have been 3-fold averaged after analysis, normalized, and contoured with the same equidistant levels. The *scale bar* represents 5 nm.

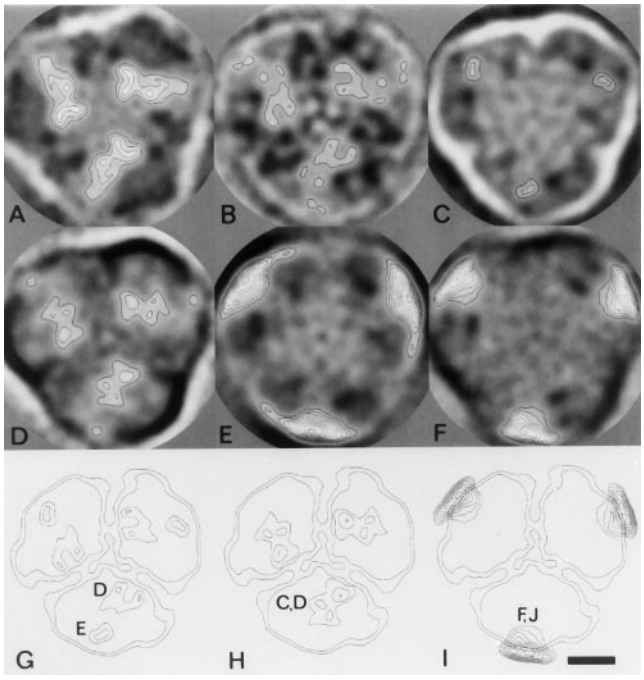

FIG. 6. **Determination of subunit positions from a comparison of the final images of trimeric top view projections by subtraction.** *A*, difference image of WT PS1 (Fig. 5*B*) and PS1 lacking PsaD/E (Fig. 5*E*). *B*, difference image of WT PS1 (Fig. 5*B*) and PS1 lacking PsaD (Fig. 5*F*). *C*, difference image of WT PS1 (Fig. 5*B*) and PS1 lacking PsaE (Fig. 5*G*). *D*, difference image of PS1 lacking PsaE (Fig. 5*G*) and PS1 lacking PsaC/D/E (Fig. 5*C*). *E*, difference image of WT PS1 (Fig. 5*B*) and PS1 lacking PsaF/J (Fig. 5*H*). *F*, difference image of WT PS1 (Fig. 5*B*) and PS1 lacking PsaJ (Fig. 5*I*). *G*, position of the subunits PsaD and PsaE (from Fig. 6, *B* and *C*, respectively). *H*, position of the subunits PsaC/D from the difference of Fig. 6*D*. *I*, position of the subunits PsaF/J (from Fig. 6*F*). All contours are on the same scale and with similar levels as in Fig. 5. In images of *A–F* the two lowest levels have been omitted (see text). The *scale bar* represents 5 nm.

only one particular area is marked (Fig. 6, *A–H*), which is consistent with only one specific subunit missing in each case.

This allowed the localization of subunits PsaC, -D, -E, -F, and -J, a localization supported by biochemical (33–35) and mutagenesis experiments (13, 30, 36, 37). Based on this set of new data we developed a model for the arrangement of the major subunits of PS1 (Fig. 7). This model will be important for the assignment of secondary structure elements as defined by the recent medium resolution x-ray structure (19, 57) to specific subunits and will be discussed in detail below.

Stromal Subunits PsaC, PsaD, and PsaE—In continuation of our previous report on stroma-side-exposed subunit of PS1, we report now the size, shape, and orientation of each individual subunit. PsaC was the only subunit to be attributed indirectly. In fact, the difference view of particles isolated from the PsaD/E deletion strain (Fig. 6*B*) with and without an attempt to rebind PsaC appear very similar to particles where PsaC/D/E have been removed by urea treatment (4). This indicates that PsaC is not present in any of these particles, which is also confirmed by SDS-PAGE (Fig. 2) and by the identical height of the corresponding side views, thus excluding a direct localization. As the individual position of PsaD and -E was obtained from separate difference maps (Fig. 6, *B–D*), it became obvious that PsaC is located in the center of the monomer, flanked by PsaD and -E. This localization was already strongly suggested by the position of the Fe-S centers $F_{A/B}$ known from the x-ray structure (19). While PsaD is located closer to the center of the trimer, PsaE is close to the periphery (Fig. 6, *G* and *H*). These data also indicate that the presence of PsaD or PsaE is necessary and sufficient to stabilize PsaC within the PS1. While an essential role of PsaD for the stabilization of PsaC has been shown previously by *in vitro* experiments (38), our data indicate that PsaD is not exclusively responsible for the stabilization of PsaC and that PsaE may play *in vivo* a major role, too (Figs. 2*D* and 6*B*) as PsaE is able to prevent the loss of PsaC. The recent functional analysis of the PsaD deletion strain reaches the same conclusion (24). The fact that a minor fraction of these particles seems to have lost PsaC/E (see Fig. 6*B*) indicates that PsaD is still needed for full stabilization of the cytoplasm-oriented subunits of PS1. As the tertiary structure of PsaC apparently is stable only under strict anaerobic conditions (38) or in the presence of PsaD/E (38), it is plausible that attempts reported in this study to rebind PsaC to PsaC/D/E-deficient complexes failed. Taken together these data suggest that PsaD is the "master" subunit, which stabilizes the whole PsaC/D/E assembly.

Measurements on various PS1 complexes (Table II) indicate that both PsaD and PsaE contribute to the absolute height of the complex and further suggest that PsaC is somewhat shielded by these two subunits. This is supported by surface accessibility studies (33, 39, 40), kinetic studies of subunit release by chaotrophic chemicals (4, 41), and the finding that PsaC is essential for rebinding of PsaD and PsaE (42). The PsaC-D cross-link induced with the zero-length cross-linker EDC (see Fig. 3) indicates a close proximity of these two subunits, which has already been suggested by cross-linking experiments with PS1 from *S. elongatus* (35) and (with a 12-Å cross-linker) in PS1 from higher plants (43). For PS1 from

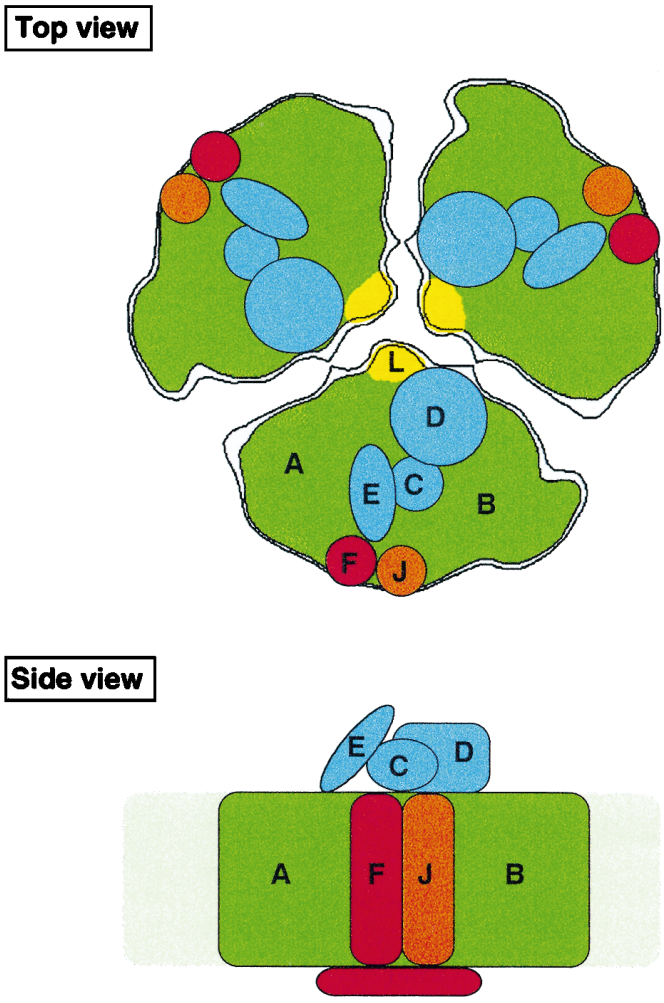

FIG. 7. **Model for the subunit arrangement in trimeric cyanobacterial PS1 as gained from EM and cross-linking experiments with WT and directed mutants.**

higher plants, cross-link products between PsaC and -E or PsaD and -E have also been reported (43, 44). The partial loss of PsaE in PS1 particles lacking PsaD (Fig. 6*B*) indicates that PsaE may shield or cover some parts of PsaD, which is also in agreement with the kinetics of subunit loss upon treatment with chaotrophic salts (4, 41, 45). As determined by NMR (46), PsaE contains a five-stranded β-sheet as main structural element, while no major helical areas could be observed. However, PsaE exhibits a loop formed by residues 42–56, which may cover PsaD while the remaining major part of PsaE is located opposite to PsaD giving rise to the difference area seen in this work for PsaE (see Fig. 6*C*).

The two iron-sulfur centers of PsaC mediate electron transport from the reaction center to the final electron acceptor ferredoxin or flavodoxin. This very efficient and fast electron transfer requires a well defined and stable positioning of PsaC, which obviously is granted by the compact, interconnected structure of the stromal subunits. Recently we showed (20, 21) that both flavodoxin and ferredoxin, despite their rather different molecular mass, use the same docking side on PS1 (20). The present subunit identification suggests that the soluble electron carriers (flavodoxin and ferredoxin) are guided and oriented by PsaE and PsaD to nearly identical docking sites. Interestingly, an antibody directed against PsaD docks at the same area of PS1 as the electron carriers do (EM data not shown), suggesting that this area apparently is optimized and most suitable for the docking of soluble proteins. These conclusions are also supported by reports showing an interaction of ferredoxin with PsaD (6, 7, 47). On the other hand, the neighborhood of ferredoxin and PsaE (Ref. 21 and this work) gives a solid structural basis for a functional role of PsaE in ferredoxin reduction as shown previously (12, 48).

PsaF and PsaJ—This paper gives for the first time strong suggestions for the localization of subunits PsaF and PsaJ close to the center of the outer edge of each monomer within the trimer. It also shows clearly that at least two membrane-spanning α-helices must be attributed to these subunits. In this position, these subunits are not shielded by other proteins, even if the monomers are aggregated in the trimeric complex; such an "exposed" position may be of significance especially for PsaF as the potential docking site for the soluble plastocyanin and/or cytochrome *c*. This "new" position is in contrast to a previously suggested, more central position for PsaF, which was derived from the low-resolving crystal structure data (18). It is in agreement, however, with the most recent structural data at 4.5 Å (19), which clearly show two or three α-helices at this position which obviously do not belong to PsaA/B and up to now could not be attributed to any subunit. While a close structural interaction between PsaF and PsaJ has already been shown (30), it is difficult to determine unambiguously from our results, which helix belongs to which subunit. We propose, however, that helix m belongs to PsaJ and helix q (for helix nomenclature, see Ref. 19) belongs to PsaF, based on the observation that the stability of PsaF is greatly reduced if PsaJ is deleted. This points to helix m as the transmembrane helix of PsaF as this helix has only minor contacts with the bulk of PS1. Also, the difference image of WT PS1 and PS1 lacking only PsaJ (on the genetic level, Fig. 6*F*) shows a higher electron density at the left side and an increase in height, which may be due to up to 30% remainder of the F subunit in these mutant particles.

The existence of at least one transmembrane α-helix per PsaF is also suggested by hydrophobicity analysis, which reveals two hydrophobic regions within this subunit (49) of which the region near the C terminus is slightly more hydrophobic. The presence of a stroma located sequence of PsaF, now evidenced by our structural data (Fig. 7), is also in agreement with the formation of a cross-link complex between PsaE and PsaF using EDC. Such a cross-link complex was also found in other cyanobacteria and in higher plants (35, 43). The existence of a hydrophobic "anchor" for PsaF was also deduced from the absence of extracted subunit upon treatment of purified PS1 with chaotropes (4, 50, 51). Finally, the side view of PS1 reveals for the first time that the F subunit, in contrast to previous assumptions, extends only in form of a very shallow disc into the lumen. In comparison with the extensive ferredoxin-docking site at the acceptor side of PS1, this supposed-to-be docking site for cytochrome c_6 and plastocyanin on the donor side seems to be much less developed. This is in line with functional measurements, showing no significant change in electron transport upon deletion of PsaF (36).

PsaL and Trimer Formation—Although not visible from our EM data, SDS-PAGE and cross-linking data from this report show the presence of PsaL in our preparation and indicate its location within PS1 in our model. The EDC cross-link product with PsaD suggests a position of PsaL close to PsaD, a structural interaction already suggested (14, 43). We moreover observed this cross-linking pattern in the monomeric as well as in the trimeric form, arguing for an intrinsic interaction between PsaD and PsaL in the monomer and not for a consequence of the trimer formation. Accordingly, this PsaD-L cross-links have also been reported for PS1 of barley (43), although up to now there is no evidence for the existence of trimeric PS1 in higher

plants. Instead higher plant PS1 contains PsaH, most likely a stromal subunit, which can be cross-linked to PsaL (43) and thus may block PsaL-PsaL interaction sterically, thereby preventing trimer formation.

In cyanobacterial PS1, PsaL was shown to be essential for trimer formation, suggesting a position at the interface of the monomers in the center of the trimer (4, 13, 52), *i.e.* next to PsaD in our model. As PS1 from a PsaD-less mutant was isolated mainly in a monomeric form lacking PsaL (see Fig. 2*D*) our results strongly indicate a significant role of PsaD, too, for the trimer stabilization. This is structurally supported by the position of PsaD extending close to the interface of the monomers (see Fig. 6, *G* and *H*).

Finally, the connecting central mass seen in our low resolution projection maps of trimeric PS1 most likely is composed of two subunits, as PsaL, with a mass of 16.6 kDa, was shown in *Synechocystis* 6803 to interact with PsaI (37), a small subunit of 4.3 kDa (1). Presumably, this mass of altogether 21 kDa, which is especially prominent in the trimers lacking PsaC/D/E (Fig. 5, *D* and *E*), forms most of the connecting masses and may represent the three α-helices observed in the central domain of the x-ray structure (19).

Comparison with Other Models—Up to now, models of subunit location within PS1 could mainly attribute subunits to a stromal, luminal, or intermembrane location (53). Also, contact sites between the stromal subunits or "nearest neighbors" could be deduced from cross-linking experiments and functional studies. However, these investigations are unable to visualize size, shape, and orientation of the respective subunits which is the prerequisite for a three-dimensional topographical model of PS1. Also, structural information on the other subunits, particularly the lumen-exposed PsaF, was lacking. Two most recently published PS1 models depict subunit interactions in cyanobacterial PS1 (3) and subunit location in higher plant PS1 (43). While the first model is based both on functional (use of deletion strains) and on cross-linking data, the latter is mainly based on an extensive cross-linking analysis. Both models integrate some of our data presented in this paper and are in agreement with them. Beyond these models, our model combines for the first time the actual structure of PS1 (as visible by EM) with the authentic three-dimensional location of individual subunits within this supercomplex.

Consequences for the Medium Resolution X-ray Structure—What new conclusions can be drawn from the EM data presented in this work in view of the medium x-ray analysis (19, 57)? Several electron density areas can now be attributed to specific subunits as outlined in detail before (PsaC, -D, -E, -F, -J, and -L). All these subunits are arranged around the central part of the two big subunits PsaA and PsaB, which also harbor the major elements of the electron transport chain. Attempts to attribute the position of these subunits relative to the position of the subunits reported here have been made. The x-ray analysis convincingly attributes all transmembrane helices, which are related by a 2-fold symmetry, to homologous subunits PsaA and PsaB (18). Recently, limited proteolysis studies have revealed that the absence of PsaD and -E expose proteolytic sites in PsaB and PsaA, respectively (54).[2] In this paper we show that PsaD is located on top of the area assigned "A" in the x-ray analysis (19). Taken together, this area in the x-ray analysis may correspond to PsaB. Alternatively, PsaA and PsaB could be more "interwoven" with each other, similar to the situation found for other membrane proteins (*i.e.* cytochrome oxidase (55)).

In conclusion, all our structural data are in line with recent reports on PS1 structure; they extend these data, however, by showing localization, shape and extension of the individual subunits within the PS1 trimer and allow their identification due to subunit-specific deletions. Fig. 7 summarizes these results by giving a three-dimensional close-to-scale schematic impression of the subunit arrangement in PS1. These data will guide and support the assignment of subunits to electron densities generated by a medium resolution x-ray analysis which could lead to a detailed structural understanding of PS1 in the near future (57).

Acknowledgments—We thank Dr. W. Keegstra for help with computer image analysis and Werner Lamkemeyer for excellent technical assistance.

[2] J. Sun and P. R. Chitnis, unpublished results.

REFERENCES

1. Bryant, D. A. (1992) in *The Photosystems: Structure, Function and Molecular Biology* (Barber, J., ed) pp. 501–549, Elsevier Science Publishers B. V., Amsterdam
2. Golbeck, J. H. (1993) *Proc. Natl. Acad. Sci. U. S. A.* **90,** 1642–1646
3. Chitnis, P. R., Xu, Q., Chitnis, V. P., and Nechushtai, R. (1995) *Photosynth. Res.* **44,** 23–40
4. Kruip, J., Boekema, E. J., Bald, D., Boonstra, A. F., and Rögner, M. (1993) *J. Biol. Chem.* **268,** 23353–23360
5. Melis, A. (1991) *Biochim. Biophys. Acta* **1058,** 87–106
6. Zanetti, G., and Merati, G. (1987) *Eur. J. Biochem.* **169,** 143–146
7. Wynn, R. M., Omaha, J., and Malkin, R. (1989) *Biochemistry* **28,** 5554–5560
8. Hippler, M., Ratajczak, R., and Haehnel, W. (1989) *FEBS Lett.* **250,** 280–284
9. Wynn, R. M., and Malkin, R. (1988) *Biochemistry* **27,** 5863–5869
10. Yu, L., Zhao, J., Mühlenhoff, U., Bryant, D. A., and Golbeck, J. H. (1993) *Plant Physiol.* **103,** 171–180
11. Sonoike, K., Hatanaka, H., and Katoh, S. (1993) *Biochim. Biophys. Acta* **1141,** 52–57
12. Rousseau, F., Setif, P., and Lagoutte, B. (1993) *EMBO J.* **12,** 1755–1765
13. Chitnis, V. P., and Chitnis, P. R. (1993) *FEBS Lett.* **336,** 330–334
14. Xu, Q., Armbrust, T. S., Guikema, J. A., and Chitnis, P. R. (1994) *Plant Physiol.* **106,** 1057–1063
15. Ford, R. C., Picot, D., and Garavito, R. M. (1987) *EMBO J.* **6,** 1581–1586
16. Almog, O., Shohmam, G., Michaeli, D., and Nechushtai, R. (1991) *Proc. Natl. Acad. Sci. U. S. A.* **88,** 5312–5316
17. Witt, I., Witt, H. T., Gerken, S., Saenger, W., Dekker, J. P., and Rögner, M. (1987) *FEBS Lett.* **221,** 260–264
18. Krauss, N., Hinrichs, W., Witt, I., Fromme, P., Pritkow, W., Dauter, Z., Betzel, C., Wilson, K. S., Witt, H. T., and Sänger, W. (1993) *Nature* **361,** 326–330
19. Fromme, P., Witt, H. T., Schubert, W.-D., Klukas, O., Saenger, W., and Krauss, N. (1996) *Biochim. Biophys. Acta* **1275,** 76–83
20. Mühlenhoff, U., Kruip, J., Bryant, D. A., Rögner, M., Sétif, P., and Boekema, E. J. (1996) *EMBO J.* **15,** 488–497
21. Lelong, C., Boekema, E. J., Kruip, J., Bottin, H., Roegner, M., and Setif, P. (1996) *EMBO J.* **15,** 2160–2168
22. Rögner, M., Nixon, P. J., and Diner, B. A. (1990) *J. Biol. Chem.* **265,** 6189–6196
23. Zhao, J., Warren, P. V., Li, N., Bryant, D. A., and Golbeck, J. H. (1990) *FEBS Lett.* **276,** 175–180
24. Hanley, J., Setif, P., Bottin, H., and Lagoutte, B. (1996) *Biochemistry* **35,** 8563–8571
25. Harauz, G., and Boekema, E. J. (1991) in *Image Analysis in Biology* (Hader, D. P., ed) pp. 196–218, CRC Press, Boca Raton, FL
26. Boekema, E. J., and Boettcher, B. (1991) *Biochim. Biophys. Acta* **1098,** 131–143
27. Harauz, G., Boekema, E. J., and van Heel, M. (1988) *Methods Enzymol.* **164,** 35–49
28. van Heel, M., and Frank, J. (1981) *Ultramicroscopy* **6,** 187–194
29. Boekema, E. J., Boonstra, A. F., Dekker, J. P., and Roegner, M. (1994) *J. Bioenerg. Biomembr.* **26,** 17–29
30. Xu, Q., Odom, W. R., Guikema, J. A., Chitnis, V. P., and Chitnis, P. R. (1994) *Plant Mol. Biol.* **26,** 291–302
31. Regnier, F. E. (1991) *Nature* **350,** 634–635
32. Tjus, S., Roobol Boza, M., Palsson, L., and Andersson, B. (1995) *Photosynth. Res.* **45,** 41–49
33. Lagoutte, B., and Vallon, O. (1992) *Eur. J. Biochem.* **205,** 1175–1185
34. Vallon, O., and Bogorad, L. (1993) *Eur. J. Biochem.* **214,** 907–915
35. Muehlenhoff, U., Zhao, J., and Bryant, D. A. (1996) *Eur. J. Biochem.* **235,** 324–331
36. Xu, Q., Yu, L., Chitnis, V. P., and Chitnis, P. R. (1994) *J. Biol. Chem.* **269,** 3205–3211
37. Xu, Q., Hoppe, D., Chitnis, V. P., Odom, W. R., Guikema, J. A., and Chitnis, P. R. (1995) *J. Biol. Chem.* **270,** 16243–16250
38. Li, N., Zhao, J., Warren, P. V., Warden, J. T., Bryant, D. A., and Golbeck, J. H. (1991) *Biochemistry* **30,** 7863–7872
39. Zilber, A. L., and Malkin, R. (1992) *Plant Physiol.* **99,** 901–911
40. Xu, Q., Guikema, J. A., and Chitnis, P. R. (1994) *Plant Physiol.* **106,** 617–624
41. Lüneburg, J., Fromme, P., Jekow, P., and Schlodder, E. (1994) *FEBS Lett.* **338,** 197–202
42. Yu, J., Smart, L. B., Jung, Y.-S., Golbeck, J., and McIntosh, L. (1995) *Plant. Mol. Biol.* **29,** 331–342
43. Jansson, S., Andersen, B., and Scheller, H. V. (1996) *Plant Physiol.* **112,** 409–420

44. Oh-oka, H., Takahashi, Y., and Matsubara, H. (1989) *Plant Cell Physiol.* **30,** 869–875
45. Chitnis, P. R., Reilly, P. A., Miedel, M. C., and Nelson, N. (1989) *J. Biol. Chem.* **264,** 18374–18380
46. Falzone, C. J., Kao, Y.-H., Zhao, J., Bryant, D. A., and Lecomte, T. J. (1994) *Biochemistry* **33,** 6052–6062
47. Lelong, C., Setif, P., Lagoutte, B., and Bottin, H. (1994) *J. Biol. Chem.* **269,** 10034–10039
48. Fromme, P., Schubert, W. D., and Krauβ, N. (1994) *Biochim. Biophys. Acta* **1187,** 99–105
49. Chitnis, P. R., Purvis, P., and Nelson, N. (1991) *J. Biol. Chem.* **266,** 20146–20151
50. Li, N., Warren, P. V., Golbeck, J. H., Frank, G., Zuber, H., and Bryant, D. A. (1991) *Biochim. Biophys. Acta* **1059,** 215–225
51. Tjus, S. E., and Andersson, B. (1991) *Photosynth. Res.* **27,** 209–219
52. Chitnis, V. P., Xu, Q., Yu, L., Golbeck, J. H., Nakamoto, H., Xie, D.-L., and Chitnis, P. R. (1993) *J. Biol. Chem.* **268,** 11678–11684
53. Golbeck, J. H. (1992) *Annu. Rev. Plant Physiol. Plant Mol. Biol.* **43,** 293–324
54. Xu, Q., and Chitnis, P. R. (1995) *Plant Physiol. (Bethesda)* **108,** 1067–1075
55. Ostermeier, C., Iwata, S., Ludwig, B., and Michel, H. (1995) *Nat. Struct. Biol.* **2,** 842–846
56. Williams, J. G. K. (1988) *Methods Enzymol.* **167,** 766–778
57. Krauss, N., Schubert, W.-D., Klukas, O., Fromme, P., Witt, H. T., Saenger, W. (1996) *Nat. Struct. Biol.* **3,** 965–973